CARBON 89 (2015) 318–327

Available at www.sciencedirect.com

ScienceDirect

journal homepage: www.elsevier.com/locate/carbon

Pressure-induced chemical enhancement in Raman scattering from graphene–Rhodamine 6G–graphene sandwich structures

Youngbin Lee [a,1], Hyunmin Kim [b,*,1], Jae-Bok Lee [c], Jeong Ho Cho [a,d], Jong-Hyun Ahn [c,*]

[a] SKKU Advanced Institute of Nanotechnology (SAINT), Sungkyunkwan University, Suwon 440-746, Republic of Korea
[b] Nano & Bio Research Division, Daegu Gyeongbuk Institute of Science and Technology, Daegu 711-873, Republic of Korea
[c] School of Electrical and Electronic Engineering, Yonsei University, Seoul 120-749, Republic of Korea
[d] School of Chemical Engineering, Sungkyunkwan University, Suwon 440-746, Republic of Korea

ARTICLE INFO

Article history:
Received 2 January 2015
Accepted 23 March 2015
Available online 30 March 2015

ABSTRACT

In this study, we introduce a new method to enhance the Raman signals of a graphene–Rhodamine 6G (R6G)–graphene sandwich structure by creating a magnet-induced static pressure to maximize the chemical contact between the R6G molecules and graphene. The increase in pressure in the graphene–R6G–graphene sandwich geometry plays a crucial role in enhancing the Raman signal by approximately up to 30 times in comparison to that acquired from a R6G/graphene layered film. In addition, the pressure-induced enhancement effects in the planar vibrational motion of the R6G (1200–1500 cm^{-1}) were more recognizable than those in the low-wavenumber region and were almost comparable to the surface-induced enhancement effects in the Raman scattering signals observed from the spontaneously formed 'folded' pseudo-π-bonded graphene–R6G–graphene sandwich structures. The enhancement effect diminished with an increase in the number of graphene layers (on the bottom side), which was clearly discernible when graphene/glass sandwiched structures placed on top of exfoliated multilayered graphene coated with R6G were imaged.

1. Introduction

Since its discovery in 1928 [1], Raman spectroscopy has been widely applied to extract chemical information from molecules. The scope of this technique ranges from the analysis of glycerol placed in a cryogenic chamber [2] to the assessment of whether water is present in the deserts of Mars [3]. However, one key challenge encountered in Raman spectroscopy is improving the scattering efficiency. Previously, attempts to overcome the limited scattering efficiency have relied on placing plasmon-inducing particles adjacent to the target molecules [4] (i.e., surface-enhanced Raman scattering, SERS), illuminating the targets with light optically tuned to the resonant frequency of the molecules [5] (resonant Raman scattering, RRS), and exposing samples to multiple light sources to create a coherent vibrational

* *Corresponding authors at:* A440 Engineering Building 1, Yonsei Univ., Seoul 120-749, Republic of Korea. Fax: +82 2 313 2879 (J.-H. Ahn). Fax: +82 53 785 3559 (H. Kim).
E-mail addresses: hyunmin.kim@dgist.ac.kr (H. Kim), ahnj@yonsei.ac.kr (J.-H. Ahn).
[1] Y. Lee and H. Kim contributed equally to this work.
http://dx.doi.org/10.1016/j.carbon.2015.03.065
0008-6223/

motion of the molecules [6] (coherent Raman scattering, CRS). Recently, graphene has been used to separate Raman spectra from a strong fluorescent background by permitting more efficient chemical contact between the fluorescent molecules and graphene substrates [7] (i.e., graphene-enhanced Raman scattering, GERS).

GERS has gained much popularity within a short period of time because it can be used to collect molecular vibrational information on fluorophores with a very simple manipulation. However, the chemical enhancement of the signals is poorly understood, although the enhancement is seemingly related to the extended charge transfer of excited electrons from fluorescent molecules to the graphene substrate [8]. In fact, the fluorescence-quenching effect of graphitic carbon was already reported for various molecules in 1994 [9]. After that, Xie et al. [10] reported the possibility of significantly reducing the fluorescent background signals from Rhodamine 6G (R6G) molecules deposited onto single-layered graphene surface by almost three orders of magnitude. Deng et al. also showed that the Raman enhancement factor of graphene–Rhodamine conjugates reached 1.7–5.6 by directly monitoring the Raman cross-section using polarization-difference resonance Raman scattering technique [11]. The degree of oxidation of the graphene oxide layer was also proved to be important for increasing the Raman intensity of the adsorbed Rhodamine B molecules [12]. Local field enhancement from well-distributed defects and spectral adjustments of molecular resonance were regarded as the possible sources of this outstanding enhancement. Optical contrast microscopy was also employed to monitor the spectral shift induced by the adsorption of R6G molecules in this study. However, despite these advantages, the Raman cross section of the R6G attached to graphene decreased to $\sim 5.1 \times 10^{-24}\ cm^2$, a threefold decrease compared to that of R6G in methanol [8].

In addition to these chemical characteristics related to Raman spectroscopy, graphene is a two-dimensional (2D) flexible sheet with excellent chemical inertness ascribed to delocalized π-bonds. Hence, graphene sheets have been frequently used to manipulate structural systems as squeezed pairs. For example, water monolayers spread on a mica surface were successfully visualized using graphene-squeezed 'coats', disclosing the dynamic nature of the ice-like behavior of water in the early stages of crystal growth [13]. In addition, the strong surface tension between the graphene layers allowed the monitoring of the formation of a platinum nanocrystalline sheet from an encapsulated liquid blister [14]. Furthermore, Fano-like hexagonal antennas covered with graphene for broadband plasmon generation were demonstrated to enhance the quantum efficiency of the photodetector by as much as ~20% [15]. Raman spectroscopy on gold nanostructures wrapped with suspended graphene allowed the direct monitoring of the spectral shift and of the enhancement in the vibrational signatures of graphene as a function of the tensile forces [16]. Very recently, a significant Raman enhancement was also achieved by inserting a dielectric layer into a metal-Rhodamine B–graphene layered system to reduce the plasmon damping [17]. However, the specific effects of the external pressure on the optical properties of molecules squeezed between graphene sheets are yet to be fully examined. In particular, the influence of the extra pressure on the charge tunneling/transfer at the graphene sandwich interface and on the subsequent enhanced Raman scattering is unknown.

In light of this, we studied the Raman spectrum of R6G sandwiched between two graphene layers in the presence of a static pressure provided by an external magnet. Using the pressure application method described here, we applied a maximum pressure of 5 kPa to verify the enhancement of most dominant Raman signals corresponding to vibrations of single-layer graphene/R6G sandwiched with a graphene/glass cover. The Raman spectra were compared by creating 2D contours to more clearly understand the role of the quenching time. We also performed pressure-enhanced Raman experiments with exfoliated graphene to critically review the role of multilayer graphene in GERS.

2. Materials and methods

2.1. Measurement system

Fig. 1 shows a schematic diagram of the experiment. All Raman measurements (excitation wavelength = 532 nm and power = ~0.5 mW at the sample, unless indicated otherwise) were performed using a commercial micro Raman system (Witec Alpha 300M+). The details of graphene synthesis by chemical vapor deposition (CVD) are described in our

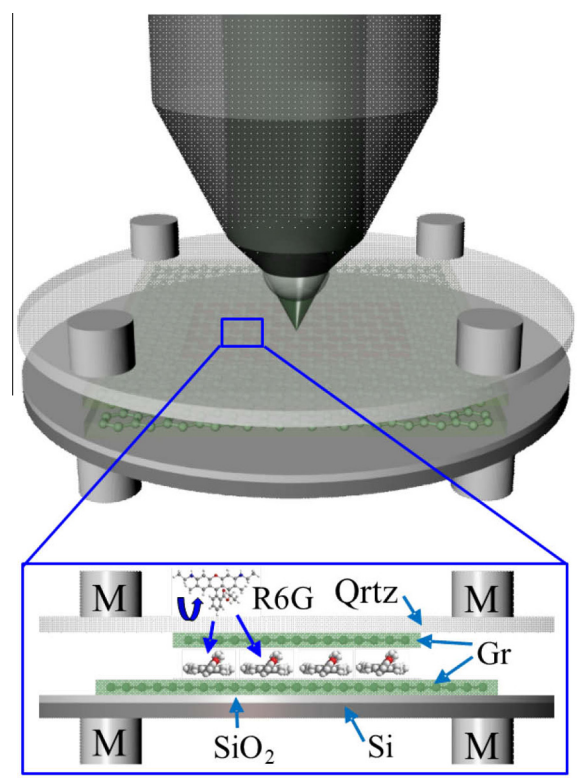

Fig. 1 – Schematic of the pressure-induced surface enhanced Raman scattering experiment. M, Niobium magnet; R6G, Rhodamine 6G dye molecule; Si, silicon; SiO_2, silicon dioxide; Gr, graphene; Qrtz, quartz glass substrate. (A color version of this figure can be viewed online.)

previous work [18]. Briefly, a vapor mixture (CH_4/H_2) was injected into an ultrahigh vacuum quartz tube to create single- to triple-layered graphene with a copper substrate also acting as the catalyst. The deposited graphene was transferred to glass and SiO_2/Si substrates to obtain the optical geometry required for Raman scattering measurements, as illustrated in the Fig. 1. R6G dye (Aldrich, 252433) was dissolved in water (0.1 μM–1 mM) and was drop-coated onto the CVD-grown and exfoliated graphene transferred to the SiO_2/Si substrate for 30 min. The substrates were then washed with water and ethanol several times. Finally, the substrate with the R6G was covered with another quartz glass slide substrate containing graphene for subsequent experiments.

2.2. *Calculation of pressure induced by magnetic force*

The pressure was loaded on the sandwich structure by using sets of cylindrical niobium magnet pairs. The magnetic flux densities of the different magnets were measured to be 0.02, 0.1, and 0.4 T (Table S1). Since the magnitudes of the magnetic fields of the magnets were different by almost an order of magnitude, an approximate value of the magnetic force was calculated from the Gilbert model [19]: $F_B = B^2A_M/2\mu_0$, where B is the magnetic flux density, A_M is the magnetized area of the magnet, and μ_0 is the permeability of the space. The maximum pressure generated by eight magnets on the glass/silicon wafer sandwich structure was calculated to be ~5 kPa according to this model. The calculated magnetic forces and pressures for the various combinations of magnets are summarized in Table S2. Extreme care was exercised to avoid any breakage of the silicon/glass wafer due to the pressure applied by the strong magnetic force (~20 N) induced by Nb magnet pairs.

3. Results and discussion

Before investigating the effects of applied pressure on GERS, we first assessed the Raman spectrum of the R6G adsorbed on single-layered graphene deposited on a silicon substrate.

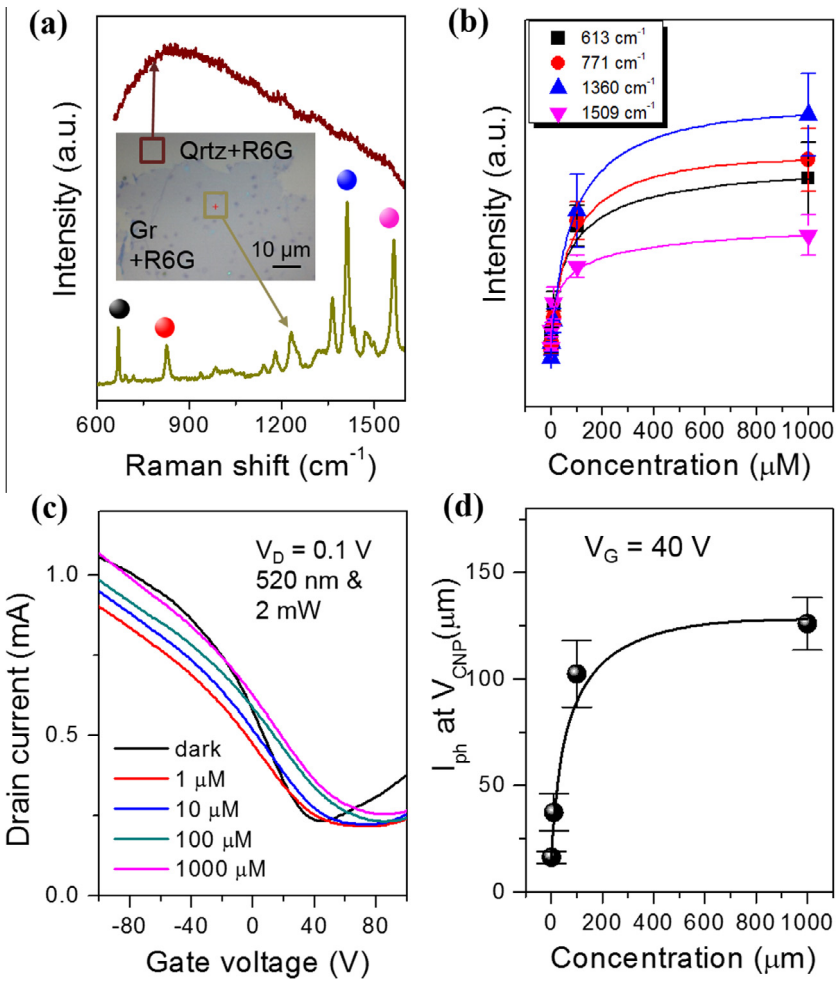

Fig. 2 – (a) Raman spectra of Rhodamine 6G (R6G) cast on the silicon substrate (brown) and single-layered graphene (dark yellow). Qrtz, quartz glass; Gr, graphene. (b) Raman intensity profile for molecular vibration states marked in (a). V_D, drain voltage. (c) Charge transfer characteristics of R6G/graphene phototransistors for various R6G concentrations. (d) Photocurrent ($I_{ph} = I_{illumination} - I_{dark}$) generated at the charge neutral point of the phototransistor as a function of R6G concentration. V_G, gate voltage. (A color version of this figure can be viewed online.)

Fig. 2a shows the Raman spectra of R6G coated onto a silicon substrate (brown) and onto a graphene layer (dark yellow). The optical image (inset) indicates the area from which each Raman signal was acquired. The measurements were acquired at least five times over an optically clean area to avoid any possibility of signal collection from aggregated R6G or R6G films on defects/multilayers of CVD-grown graphene layers.

The spectra were taken for 100 s to achieve a good signal to noise ratio (S/N > 20). The spectra from R6G coated on the graphene surface (dark yellow) were clearly resolved, whereas those from R6G coated directly onto the silicon substrate were poorly resolved (brown). This trend agreed well with previous reports [10].

The concentration dependence of the R6G solution was also studied to confirm the reliability of the molecular dispersion over the surface, as shown in Fig. 2b. As shown, a relatively higher concentration (>100 μM) was required to achieve saturation in the Langmuir-type isotherm curve than was previously reported (<10 μM) [10], probably because of the large surface area (~1 cm^2) of graphene deposited by CVD. The concentration dependence of the Raman intensity for different molecular vibration states of R6G is shown in Fig. S1.

A phototransistor measurement of the R6G/graphene hybrid channel was also conducted to monitor the charge transport in the GERS process, from which ensemble-level uniformity of the R6G molecular distribution over the graphene surface could be assessed. The schematic device structure of the R6G/graphene hybrid phototransistor and the observed electronic properties are represented in Fig. S2. Fig. 2c shows the total drain current (dark plus photoinduced current) of the phototransistor for various R6G concentrations in the range of 1 to 1000 μM. The photocurrent ($I_{ph} = I_{illumination} - I_{dark}$) [20] was measured at a fixed drain voltage (0.1 V), fixed incident illumination wavelength (520 nm), and fixed power (1 mW). The charge neutral point (CNP) of the phototransistor was located at 40 V and shifted to larger positive gate voltage values with the addition of R6G molecules. The total drain current at the CNP is also summarized for various R6G concentrations in Fig. 2d. As was somewhat expected, the photocurrent changes with R6G concentration had a tendency similar to that of the Langmuir-type isotherm curve (beta spline) in Fig. 2b. The mechanism of this photocurrent generation in this R6G/graphene hybrid system can be explained as follows; the electrons transferred from graphene to the R6G HOMO level recombine with photoexcited holes, and the accumulation of photoexcited electrons by R6G molecules offers more effective photogating that produces a positive shift in CNP and a high photocurrent at the CNP of the dark state [20]. More specifically, the π-bond between R6G and graphene can promote the stacking of the photoexcited electrons at R6G layer, allowing a high level of hole movement within the graphene layer mimicking an effective gate behavior. The photocurrent could be increased by pumped hole carriers from source electrode, which is arouse from effective photogating of photo-excited electrons in the dye layer. Also, the photo-induced difference in the chemical potential enhances the charge tunneling efficiency from graphene to the R6G LUMO level associated with the extremely high carrier mobility in graphene (~1000 cm^2/V s), which drastically hampers an electron–hole recombination process in the dye layers. Additionally, the reduced recombination time in dye layer plays a critical role in enhancing the effective quantum efficiency to the level of ~10^5% since the photocurrent gain is determined by the ratio between the electron relaxation time (an order of millisecond) in the dye layer and the carrier transit time (an order of picosecond) in the graphene layer. We also note a positive correlation between the Raman signal and photocurrent as functions of the laser power in Fig. S3, which reveals the role of charge transfer in the chemical enhancement of Raman scattering in GERS.

To understand the effect of the static load on the chemically enhanced Raman scattering more deeply, it is important to define the enhancement factor related to the change in the Raman cross section induced by the graphene/glass cover. Two decisive factors affecting the Raman scattering cross section are the reflectivity at the interfaces and the solid angle (Ω). A beam linearly polarized along the *x*-direction in the lens plane can be recategorized using a ratio between *s* (azimuthal direction in the lens plane) and *p* polarization (radial direction in the lens plane) for the sake of interpretation (inset in

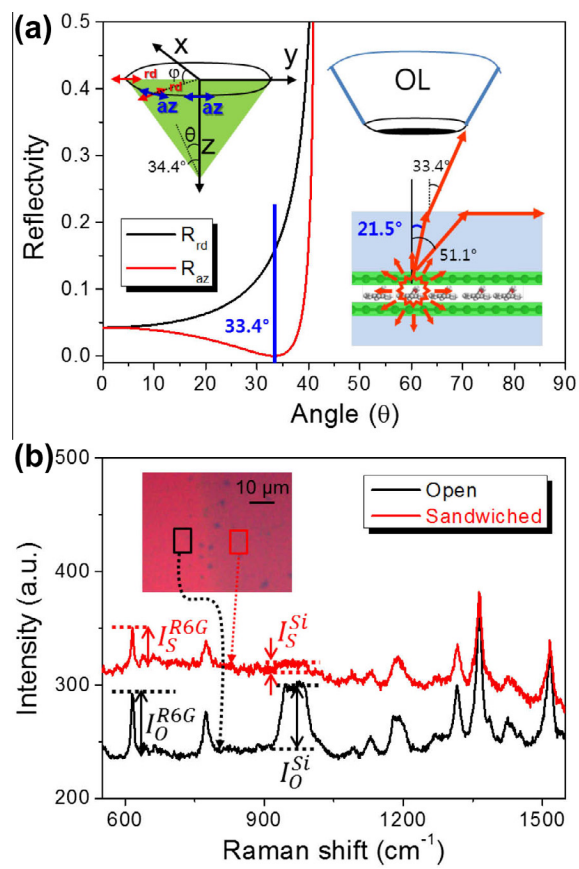

Fig. 3 – (a) Reflectivity of *s*- and *p*-polarized light as a function of the angle of the incident beam. The inset figure depicts the difference in the collection solid angle of the generated Raman scattering in the presence and absence of the 'graphene cover'. (b) Scheme for calculating the Raman enhancement factor of R6G molecules in the sandwiched condition with respect to the open condition in Eq. (2). (A color version of this figure can be viewed online.)

Fig. 3a). We note that the incident beam still contained ~90% of the x-direction component after it passed through an objective lens with a numerical aperture of 0.55 [21]. The Fresnel reflectances for the s- and p-polarized beams as a function of the incident angle (θ) in an air/glass system are shown in Fig. 3a, where n_a and n_g are the refractive indices of air and glass, respectively. The theoretical average transmittance between air and glass at incidence angles in the range 0–33.4° (NA = 0.55) is ~0.953 [22]. Thus, the total transmittance of the graphene/glass cover can be approximated as 0.924 considering the transmittance of single-layered graphene, which is quite close to the value obtained experimentally using a power meter (~0.93).

During scattering, the graphene/glass cover cuts the outermost angle of the outgoing beam from 33.4° to 21.5°, as illustrated in the inset, reducing the collection efficiency by 64.6%. The thickness of the graphene layer was not considered while evaluating this angular difference, and we note that total internal reflection occurs at 51.1°. This information allowed us to take a more quantitative approach to evaluating the chemical enhancement factor of the R6G Raman signals attributable to the graphene/glass cover. We first assumed that the number density of R6G molecules (i.e., 6.4×10^{13} cm^{-1}) [23] was identical regardless of the existence of the graphene/glass cover.

According to the literature [24], the differential Raman cross section ($d\sigma/d\Omega$) of a vibrational mode of a molecule (e.g., a carbon nanotube, CNT) on a silicon substrate can expressed as follows:

$$\left(\frac{d\sigma}{d\Omega}\right)^{\text{v.mode}} = I^{\text{CNT}}_{\text{v.mode}}/I^{\text{Si}} \cdot d\Sigma/d\Omega \cdot A \quad (1)$$

Here, the I values indicate the Raman intensities, $d\sum/d\Omega$ is the apparent Raman cross section of the Si substrate (in sr^{-1}), and A is the size of the laser spot. We used the first overtone peak (900–1000 cm^{-1}) of Si Raman scattering, because it is not saturated under our data collecting conditions. On the basis of the above information, we can calculate the chemical enhancement factor attributable to the graphene/glass cover (EF) as follows [25]:

$$EF = \frac{(d\sigma/d\Omega)^{\text{R6G}}_{\text{S}}}{(d\sigma/d\Omega)^{\text{R6G}}_{\text{O}}} = \frac{I^{\text{R6G}}_{\text{S}}/I^{\text{Si}}_{\text{S}} \cdot (d\Sigma/d\Omega)_{\text{S}} \cdot A}{I^{\text{R6G}}_{\text{O}}/I^{\text{Si}}_{\text{O}} \cdot (d\Sigma/d\Omega)_{\text{O}} \cdot A} = \frac{I^{\text{R6G}}_{\text{S}}/I^{\text{Si}}_{\text{S}}}{I^{\text{R6G}}_{\text{O}}/I^{\text{Si}}_{\text{O}}} \cdot SF \quad (2)$$

Here, the values for $I^{\text{R6G}}_{\text{O}}$, I^{Si}_{S}, and I^{Si}_{O} are graphically depicted in Fig. 3b (S, sandwich; O, open); SF corresponds to the ratio between the two (sandwiched and open) apparent Raman cross sections stemming from the structural factor. The concept of the apparent Raman cross section was adopted here because it is an inherent property defined for Si. We did not attempt to calculate the cross section directly; instead, we attempted to obtain the enhancement ratio created by the difference in the collection efficiency, in the form of the SF. The EF can be expressed by multiplying the transmittance and the solid angle change, which yields approximately 2–5.

Fig. 4a shows the 2D contour diagrams of the Raman spectra extended to the time scale for the R6G-adsorbed single-layered graphene system without (open) and with the graphene/glass cover (sandwiched), subjected to a pressure of 5 kPa. The spectra were acquired simultaneously with the laser light switched on for 1 s for a period of 100 s. A noticeable peak was found to arise in the background when the graphene/glass cover was applied.

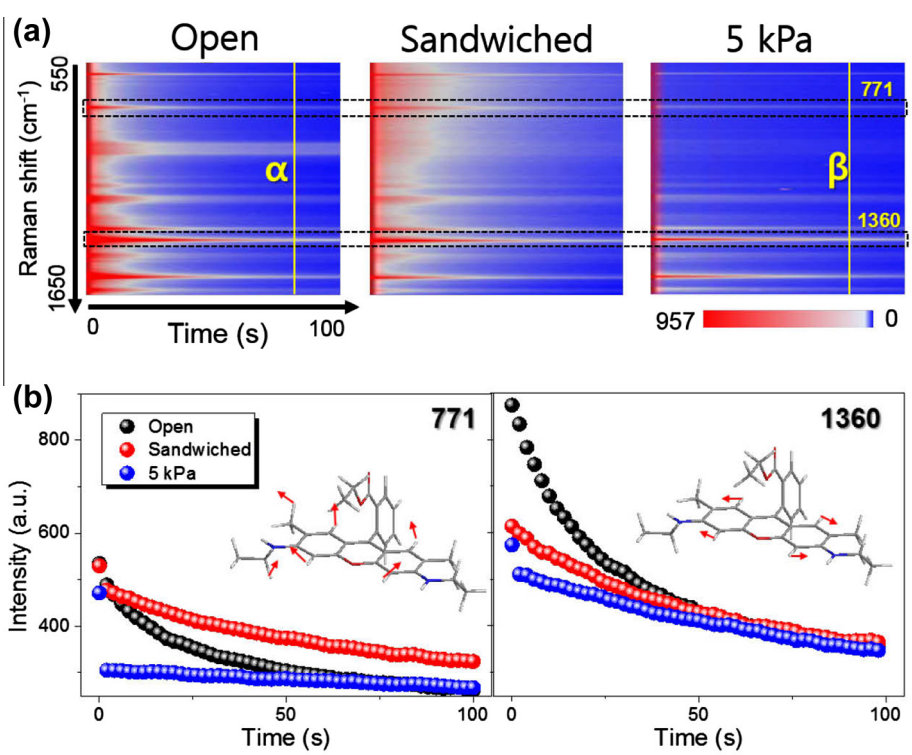

Fig. 4 – Time dependent (a) 2D contour Raman spectra and (b) intensity decay profiles for molecular vibration states (771 cm^{-1} and 1360 cm^{-1}) for open, sandwiched, and pressured (5 kPa) conditions. (A color version of this figure can be viewed online.)

The broad background peak (500 cm^{-1}–1000 cm^{-1}) loosely overlapped with the location of R6G fluorescence emission (at ~550 nm in a wavelength scale by 532 nm excitation), which remarkably disappeared under the static load (of 5 kPa). We believe that the superfluous fluorescence generated by the extra electron–hole recombination in the graphene sandwich structure leads to electron transfer to the neighboring graphene layer, given that the applied pressure results in a higher contact area. The time-dependent profiles of two representative vibrations (out-of-plane C–H bending at ~771 cm^{-1} and aromatic C-C stretching at ~1360 cm^{-1}) [26] are redrawn in Fig. 4b to provide a clearer understanding of the changes in the fluorescence and Raman spectra. The slight spectral shift associated with the applied pressure was not considered in this work. A more qualitative comparison of the data sets was achieved by redrawing the time constants (τ) from the exponential decay model ($I = I_0 e^{-t/\tau}$), which were fitted to 28.9 s (open), 57.7 s (sandwich), and 65.1 s (5 kPa) for the peak at 771 cm^{-1} and 29.2 s (open), 59.2 s (sandwich), and 64.7 s (5 kPa) for the peak at 1360 cm^{-1}. The meaning of time constant here will be the extent of time-dependent signal change according to the photobleaching of R6G dye, which would be frequently met in the laser induced fluorescence measurement. The values were similar for identical sample conditions regardless of the kind of vibration, although a clear difference was observed between fluorescence-dominant (open) and Raman-dominant (5 kPa) spectra. As mentioned earlier, the abrupt intensity changes (within 2 s) observed under pressure could be attributed to an instantaneous high level of fluorescence quenching occurring in the highly squeezed condition. It is noteworthy that the fluorescence at 771 cm^{-1} (not 1360 cm^{-1}) remained under the sandwiched condition and was confirmed as a 'pseudo-stimulated' fluorescence emission created by the graphene cover.

The effect of the static load on the chemical enhancement of the R6G Raman spectra is illustrated in Fig. 5a by comparison with spectra acquired from a 'folded' area generated naturally during sample preparation (shown as the region enclosed in a square in the inset optical image). Strong Raman signals of R6G were repeatedly measured from this kind of folded area, similar to the strong Raman signals from low-concentration CuPc [copper (II) phthalocyanine] doped to double-layered graphene reported in the literature [27]. When the graphene layer grown by CVD is folded, the hexagonal lattices of the upper and lower layers are randomly oriented, unlike in multilayered graphene exfoliated from graphite with a regular stacking sequence between layers [28]. As a result, stacking or folding in multilayered graphene is associated with improved electrical conductivity without any significant change in the electronic band structures. In addition, a graphene film grown by CVD generally includes defects such as pinholes and microcracks created during the synthesis and transfer process. Such defects are detrimental to the inherent advantageous properties of graphene and can also have an influence on the Raman signals, but upon folding, the upper-layer graphene can cover the defects in the lower-layer graphene, thus restoring graphene's properties. These are the main factors that result in the enhanced Raman signals from folded graphene layers. Spectra α and β were acquired 80 s after the start of the measurement so that any possible difference in the fluorescence between the two could be ignored. The effect of pressure on Raman scattering was more prominent for the in-plane motion of the molecules (1250–1600 cm^{-1}) than for the out-of-plane C–H bending (~771 cm^{-1}) or the deformation of the xanthene ring (~613 cm^{-1}). The tendency was also analyzed more quantitatively, as shown in Fig. 5b, which indicates 1–2-fold enhancements for the peak at 771 cm^{-1} and 3–4-fold enhancements for the peak at 1360 cm^{-1}. These results can be combined with the calculated enhancement factor obtained previously to extract the pressure-induced Raman enhancement factors. The factors were found to be 2–14 for the peak at 771 cm^{-1} and 6–28 for the 1360 cm^{-1} peak. The sample-to-sample variation was quite large under higher pressures, which could be ascribed to the uneven distribution of the molecules, to the pressure induced by the bending of the silicon/glass substrate and the associated formation of an irregular stress field, and to imperfection in the graphene layer.

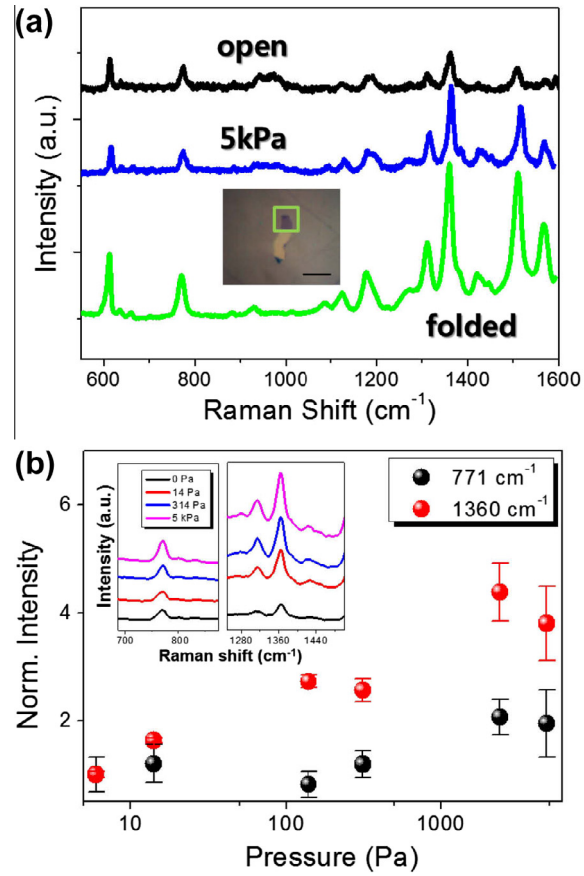

Fig. 5 – (a) Raman spectra under open (α) and pressured (β) conditions taken 80 s after signal acquisition. A spectrum from the folded area is presented for comparison. The scale bar in the inset picture corresponds to 10 μm. (b) Pressure dependence of Raman peak intensities, where the inset Raman spectra show the pressure dependence of the two vibration states (771 cm^{-1} and 1360 cm^{-1}). (A color version of this figure can be viewed online.)

The dependence of the chemically enhanced Raman scattering of R6G on the number of graphene layers in the bottom layer of the graphene–R6G–graphene system was also studied.

The number of graphene layers was determined using the optical contrast of a microscopic image and differences in the intensity ratio (I_{Gmode}/I_{2Dmode}) of major Raman peaks for graphene (Fig. S4). In order to prove the effect of graphene, we have compared Raman spectra of pressured R6G molecules on graphene and graphite. As shown in Fig. S5, graphene causes a stronger enhancement of the Raman signal and produces a clearer pressure effect than graphite. For a clear analysis, we used exfoliated graphene layers on which 100 μM of R6G molecules in water were drop-coated for 30 min. Fig. 6a shows the optical image for an area of the graphene–R6G–exfoliated-graphene system containing 1–4 layers of graphene within a single optical view, and Fig. 6b and c are Raman mappings over the same region. Raman mapping was carried out with the application of 5 kPa of pressure at (b) 771 cm^{-1} and (c) 1360 cm^{-1}. A clear difference in the Raman contrast was observed for different numbers of layers, with the highest Raman intensity seen for the graphene/R6G/single-layered graphene structure. Almost no enhancement was observed for the graphene/R6G/four-layer graphene systems. This can also be observed in the Raman intensity line profile (Fig. 6d) along the dotted lines in Fig. 6b and c, where the intensity increased almost linearly with a decrease in the number of graphene layers from the four-layer sample to the single-layer sample. According to the literature [29], Langmuir–Blodgett (LB) films of adsorbed fluorescent molecules only play a critical role in facilitating the charge transfer to the graphene layer if the LB film is in direct contact with the graphene. This is true regardless of the number of layers in the LB film or whether the graphene layer is located above or below the LB film. In the graphene sandwich structure, the *inserted* R6G film should be the nearest ('first') R6G layer for both graphene substrates, and thus it will be 'counted' twice as a source of charge transfer and thus chemical enhancement. Furthermore, static pressure might *squeeze* out electrons from the R6G layers, leading to an enhancement in the Raman scattering efficiency due to accelerated tunneling of the carriers. A suggestive analogous phenomenon to this enhancement in charge transfer by pressure is piezoelectricity or piezo(mechano)luminescence, where abrupt tunneling of carriers is followed by spontaneous electron–hole recombination [30].

An identical trend with decreasing number of graphene layers was observed in the Raman mapping data obtained without pressure, although the overall intensity was lower. This observation is quite different from some previous results reporting superior Raman enhancement by double-layered graphene systems [27] or reporting a drastic decrease in

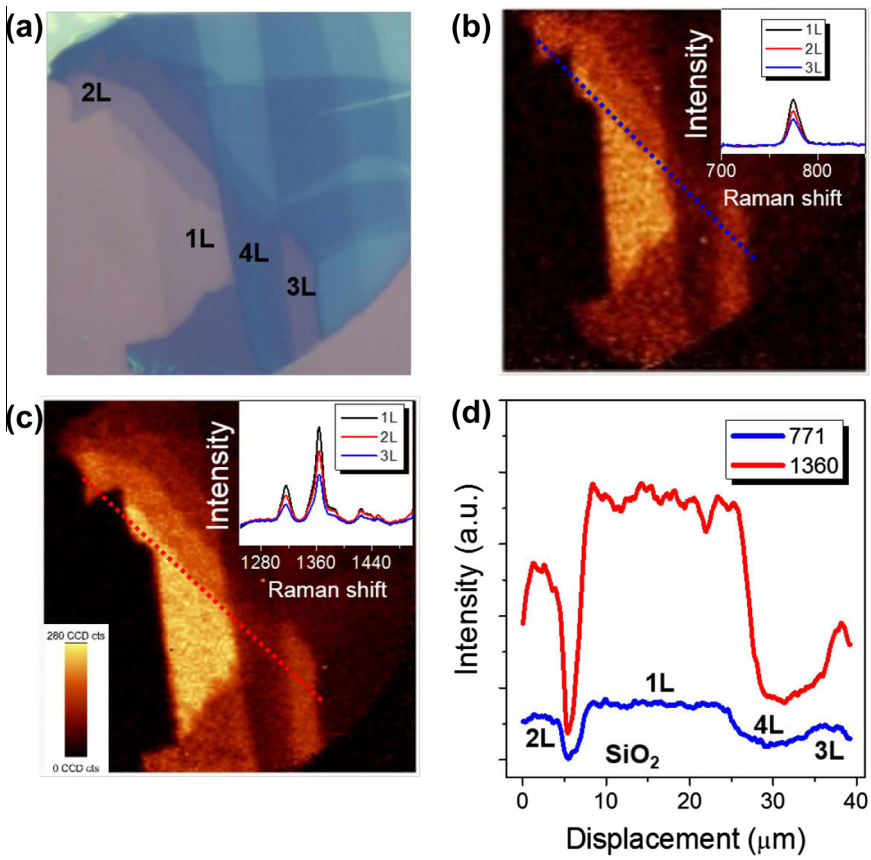

Fig. 6 – (a) Optical micrograph and Raman mapping images of samples maximally (5 kPa) pressured at (b) 771 cm^{-1} and (c) 1360 cm^{-1} for exfoliated graphene with different numbers of layers coated with R6G molecules. Raman spectra from single, double, and triple layered graphene are summarized in the inset spectrographs in (b) and (c), respectively. The units of the inset graphs for intensity and Raman shift are arbitrary and cm^{-1}, respectively. (d) Raman intensity profiles along the dotted lines in (b) and (c). (A color version of this figure can be viewed online.)

the Raman intensity from single- to double-layered systems [31].

We also observed that the Raman intensity ratios among the systems with different graphene thicknesses were the same at 1360 cm^{-1} or at 771 cm^{-1}, even though the intensity at 1360 cm^{-1} was higher than that at 771 cm^{-1}. The quantitative pressure dependence of the Raman signals is summarized in Fig. 7a and b for the peaks at 771 cm^{-1} and 1360 cm^{-1}, respectively. The enhancement factor of around 2 in the single-layered system decreased to almost 1 in the three-layered system. We also note that in the graphene–R6G–multiple-graphene structures, only the two graphene layers actually in contact with the R6G film act as 'first' layers to create a high level of chemical enhancement. As the number of graphene layers increases, the Raman signals tend to decrease (in particular, at high pressure), in contrast to the case for folded graphene layers. This is in good agreement with the trend observed for dye adsorption on graphene by solvent soaking [31], although some opposite trends have also been observed, especially in few-layered systems. For example, the opposite trend was observed for thermally grown low-concentration PPP (protoporphyrin IX) films covered with transferred graphene layers [27] and for intercalated iodine ions [32]. To explain these differences, we believe that the different work function of multilayered graphene and the different surface potential induced by the SiO_2/Si substrate [7] affect the quality of the electron transfer and that untraceable optical effects might hamper the data collection efficiency [8]. In particular, the graphene multilayer exfoliated from graphite exhibits a regular stacking sequence of layers, which causes a change in the electronic band structure due to the interaction between layers, in contrast to CVD-grown graphene. These changes can in turn lead to the tailoring of the Raman signals as well as a subsequent chemical enhancement induced by pressure. Based on the experiments using thermal evaporation-assisted deposition of R6G coatings to obtain a more solid chemical contact between the dyes and layered graphene, Ling et al. concluded that chemical enhancement of Raman signals can also occur through electron tunneling from (and to) energy states (HOMO and LUMO) created by doped R6G molecules. In fact, we also applied a similar idea to create a broadband atmospheric photodetector and successfully adapted the R6G-doped graphene (and MoS_2) system as an excellent tool for creating an ultrahigh-signal-response photodetector [20]. In addition, a supportive Raman spectroscopy/imaging study on crystal violet, Rhodamine B, and protoporphyrin IX dyes is included in Figs. S7 and S8 to show the differences in the pressure-induced enhancement compared with that found in the R6G–graphene system.

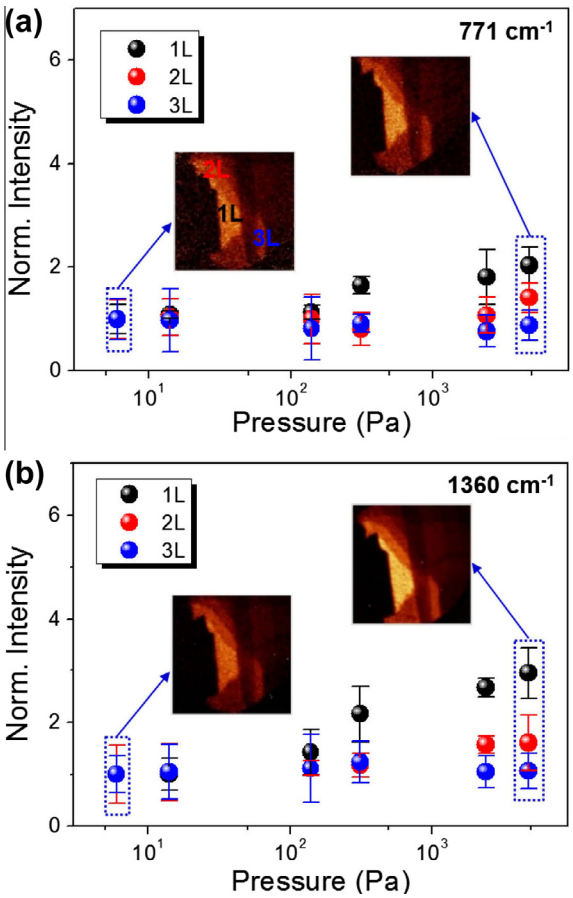

Fig. 7 – Pressure dependence of Raman signals at (a) 771 cm^{-1} and (b) 1360 cm^{-1} of R6G sandwiched by single-layered graphene and single-, double-, or triple-layered graphene on an Si substrate (Intensities were normalized against the intensity of unpressurized case). Thumbnail images are representative Raman intensity mapping images for the pressure conditions corresponding to the indicated dotted squares. (A color version of this figure can be viewed online.)

4. Conclusion

In summary, we studied the chemical enhancement of Raman signals of strongly fluorescent R6G molecules sandwiched between two graphene layers in combination with static loading of this structure using Nb magnets with a pressure up to ~5 kPa. The Raman intensity was enhanced by 10–30 times by the application of pressure to the graphene–R6G–graphene sandwich structure, in comparison to the intensities observed in the case of the R6G–graphene system without sandwiching. The two main factors causing this significant enhancement are the improved chemical contact and pressure-induced-quenching of the high fluorescent background, which give rise to clearer vibrational signals. The improved chemical contact mainly enhances the Raman intensity through double counting of the R6G film, which acts as a 'first layer' for both graphene films in the sandwiched structure. The pressure-induced-quenching might occur through acceleration of carrier transfer when the sandwich is pressed, similar to that occurring in piezoelectricity. The largest pressure effect on the chemical enhancement might be achieved in a folded graphene structure, which is a synthetic analogue of CVD-synthesized R6G/graphene double layers in which the contact between R6G and graphene is controlled at the atomic scale. An increase in the number of graphene layers in the sandwich structure (in either the presence or absence of pressure) led to a decrease in the enhancement in the Raman intensity, in agreement with previous results for

solvent-mediated dye adsorption on single- and multiple-layered graphene. In this study, we did not consider the effects of the nano/microstructural morphology of the coated R6G in GERS, which might be significant. Nonetheless, we still believe that our work paves the way for studying dynamically controlled chemical contact in GERS. In this light, a current ongoing project focuses on the Raman spectroscopy of dye molecules in a sandwiched graphene geometry where static loading is activated by magnetic nanoparticles. This provides a more programmed source for the chemical enhancement of the vibrational peaks. Much further research is required to understand the details of GERS in different materials, specifically with regard to the quality of the physical contact and correlation with external fields.

Acknowledgments

H.K. acknowledges the provision of the basic research programs (14-NB-04) and a start-up fund for new researchers through the Daegu Gyeongbuk Institute of Science and Technology (DGIST) funded by the Ministry of Science, ICT, and Future Planning of Korea. J.-H.A. acknowledges the Research Program (CASE-2014M3A6A5060933 and 2009-0083540) through the National Research Foundation of Korea (NRF), funded by the Ministry of Science, ICT, and Future Planning of Korea.

Appendix A. Supplementary data

Supplementary data associated with this article can be found, in the online version, at http://dx.doi.org/10.1016/j.carbon.2015.03.065.

REFERENCES

[1] Raman CV, Krishnan KS. A new type of secondary radiation. Nature 1928;121:501–2.
[2] Mendelovici E, Frost RL, Kloprogg T. Cryogenic Raman spectroscopy of glycerol. J Raman Spectrosc 2000;31:1121–6.
[3] Pérez FR, Martinez-Frias J. Raman spectroscopy goes to mars. Spectrosc Eur 2006;18:18–21.
[4] Jeanmaire DL, van Duyne RP. Surface Raman electrochemistry part I. Heterocyclic, aromatic and aliphatic amines adsorbed on the anodized silver electrode. J Electroanal Chem 1977;84:1–20.
[5] Schmitt M, Popp J. Raman Spectroscopy at the beginning of the twenty-first century. J Raman Spectrosc 2006;36:20–8.
[6] Tolles WM, Nibler JW, McDonald JR, Harvey AB. A review of the theory and application of coherent anti-stokes Raman spectroscopy (CARS). Appl Spectrosc 1977;31:253–71.
[7] Ling X, Xie L, Fang Y, Xu H, Zhang H, Kong J, et al. Can graphene be used as a substrate for Raman enhancement? Nano Lett 2010;10:553–61.
[8] Thrall ES, Crowther AC, Yu Z, Brus LE. R6G on graphene: high Raman detection sensitivity, yet decreased Raman cross-section. Nano Lett 2012;12:1571–7.
[9] Kagan MR, McCreery RL. Reduction of fluorescence interference in Raman spectroscopy via analyte adsorption on graphitic carbon. Anal Chem 1994;66:4159–65.
[10] Xie L, Ling X, Fang Y, Zhang J, Liu Z. Graphene as a substrate to suppress fluorescence in resonance Raman spectroscopy. J Am Chem Soc 2009;131:9890–1.
[11] Deng S, Xu W, Wang J, Ling X, Wu J, Xie L, et al. Direct measurement of the Raman enhancement factor of Rhodamine 6G on graphene under resonant excitation. Nano Res 2014;7:1271–9.
[12] Huh S, Park J, Kim YS, Kim KS, Hong BH, Nam J-M. UV/ozone-oxidized large-scale graphene platform with large chemical enhancement in surface-enhanced Raman scattering. ACS Nano 2011;5:9799–806.
[13] Xu K, Cao P, Heath JR. Graphene visualizes the first water adlayers on mica at ambient conditions. Science 2010;329:1188–91.
[14] Yuk JM, Park J, Ercius P, Kim K, Hellebusch DJ, Crommie MF, et al. High-resolution EM of colloidal nanocrystal growth using graphene liquid cells. Science 2012;336:61–4.
[15] Fang Z, Liu Z, Wang Y, Ajayan PM, Nordlander P, Halas NJ. Graphene-antenna sandwich photodetector. Nano Lett 2012;12:3808–13.
[16] Heeg S, Fernandez-Garcia R, Oikonomou A, Schedin F, Narula R, Maier SA, et al. Polarized plasmonic enhancement by au nanostructures probed through Raman scattering of suspended graphene. Nano Lett 2012;13:301–8.
[17] Yu X, Tao J, Shen Y, Liang G, Liu T, Zhang Y, et al. A metal-dielectric-graphene sandwich for surface enhanced Raman spectroscopy. Nanoscale 2014;6:9925.
[18] Lee Y, Bae S, Jang H, Jang S, Zhu S-E, Sim SH, et al. Wafer-scale synthesis and transfer of graphene films. Nano Lett 2010;10:490–3.
[19] Griffiths DJ, College R. Introduction to Electrodynamics, vol. 3. Upper Saddle River, NJ: Prentice Hall; 1999.
[20] Yu SH, Lee Y, Jang SK, Kang J, Jeon J, Lee C, et al. Dye-sensitized MoS_2 photodetector with enhanced spectral photoresponse. ACS Nano 2014;8:8285–91.
[21] Saito Y, Kobayashi M, Hiraga D, Fujita K, Kawano S, Smith N, et al. z-Polarization sensitive detection in micro-Raman spectroscopy by radially polarized incident light. J Raman Spectrosc 2008;39:1643–8.
[22] No perceivable difference was found between this value and the one for considering single-layered graphene (thickness: 0.355 nm, n: 2.711+1.35i) from the calculation based on the multilayered Fresnel system in the literature. (W.N. Hansen, JOSA 1968, 58, 380–388).
[23] Iyi N, Sasai R, Fujita T, Deguchi T, Sota T, López Arbeloa F, et al. Orientation and aggregation of cationic laser dyes in a fluoromica: polarized spectrometry studies. Appl Clay Sci 2002;22:125–36.
[24] Bohn JE, Etchegoin PG, Le Ru EC, Xiang R, Chiashi S, Maruyama S. Estimating the Raman cross sections of single carbon nanotubes. ACS Nano 2010;4:3466–70.
[25] Pavel IE, Alnajjar KS, Monahan JL, Stahler A, Hunter NE, Weaver KM, et al. Estimating the analytical and surface enhancement factors in surface-enhanced Raman scattering (SERS): a novel physical chemistry and nanotechnology laboratory experiment. J Chem Educ 2011;89:286–90.
[26] Hildebrandt P, Stockburger M. Surface-enhanced resonance Raman spectroscopy of Rhodamine 6G adsorbed on colloidal silver. J Phys Chem 1984;88:5935–44.
[27] Ling X, Wu J, Xie L, Zhang J. Graphene-thickness-dependent graphene-enhanced Raman scattering. J Phys Chem C 2013;117:2369–76.
[28] Bae S, Kim H, Lee Y, Xu X, Park J-S, Zheng Y, et al. Roll-to-roll production of 30-inch graphene films for transparent electrodes. Nat Nanotechnol 2010;5:574–8.

[29] Ling X, Zhang J. First-layer effect in graphene-enhanced Raman scattering. Small 2010;6:2020–5.
[30] Jeong SM, Song S, Joo K-I, Kim J, Hwang S-H, Jeong J, et al. Bright, wind-driven white mechanoluminescence from zinc sulphide microparticles embedded in a polydimethylsiloxane elastomer. Energy Environ Sci 2014;7:3338–46.
[31] Qiu C, Zhou H, Yang H, Chen M, Guo Y, Sun L. Investigation of *n*-layer graphenes as substrates for Raman enhancement of crystal violet. J Phys Chem C 2011;115:10019–25.
[32] Jung N, Crowther AC, Kim N, Kim P, Brus L. Raman enhancement on graphene: adsorbed and intercalated molecular species. ACS Nano 2010;4:7005–13.